Scientific Research Publishing

Monte Carlo Study of 3D Stray Radiation during Interventional Procedures

Khalid S. Alzimami

Department of Radiological Sciences, College of Applied Medical Sciences, King Saud University, Riyadh, KSA

Email: kalzimami@ksu.edu.sa

Abstract

In interventional medical procedures, other than the highly important issue of optimizing image quality and patient exposure using the primary beam, there remains a continuing need for the study of staff exposure from the scattered radiation. Herein, investigation is made of the 3D stray-radiation distribution, the simulation being made of a realistic interventional scenario through use of the Monte Carlo code Geant4 (version 10.3). The simulation is conducted based on the high definition reference Korean-man (HDRK-man) computational phantom and a GE Infinia 3/8" C-arm machine, focusing on the effect of variation of kVp and field of view (FoV) on the scattered particles' spatial distribution. With direct measurement of the absorbed dose remaining challenging, not least in respect of the organs at risk, we computed the scatter fractions, defined as the ratio of the air kerma free-in-air to the entrance surface air kerma (ESAK), which are both easily quantifiable. Scatter fraction distributions were simulated for X-ray tube outputs (and half-value layers, HVL) of 60 kVp (2.3 mm Al), 80 kVp (3.2 mm Al) and 120 kVp (4.3 mm Al) and FoV of 15, 20, 25 and 30 cm. The distributions are obtained for different height levels, corresponding to the lens of the eye, and the lung and prostate, all radiosensitive organs. Investigations are made for eight likely locations around the patient. At fixed FoV results reveal an inverse relationship between ESAK and kVp, also that change in kVp from 60 to 80 has a greater effect than from 80 to 120. For change in FoV at fixed kVp, the scatter fraction remains constant. The particular staff locations are found to be optimal in seeking mitigation of dose. Moreover, the combined usage of numerical human model and Monte Carlo simulation can be considered as an added value to the radiation safety research field, especially to the interventional radiology staff and to the patient.

Keywords

Stray Radiation, Interventional Procedures, Operator Exposure, Geant4

1. Introduction

Interventional radiology (IR) and cardiology (IC) are of undoubted value in the diagnosis and treatment of diseases, their efficacy being reflected in the growing availability of these procedures within many larger medical centers throughout the world. The procedures are conducted by a team of medical staff who during the intervention all remain within the specialized theatre, typically being in close proximity to the patient. Given that such live-time imaging procedures are typically of protracted duration, it is of no surprise that when compared to other frequent radiological methods, IR and IC represent two of the most significant in terms of radiation exposure to medical staff. Although perhaps obvious, it is nevertheless worth noting that with the ever-increasing demand for the conduct of such procedures there comes an associated increase in radiation exposure to staff. *A priori* knowledge of the occupational absorbed dose to such staff can assist in keeping exposure levels as low as reasonably achievable [1]. Of interest is that previous success in maintaining levels below the dose limit has not always prevented cataract formation, with incidences of brain cancer among radiologists also being suggested as being implicated [2] [3] [4] [5] [6]. As such, computational-exposure scenarios mimicking realistic interventional procedures are important in predicting the 3D scatter (stray) radiation arising from the patient and apparatus. Over the last decade, investigations of patient and staff exposure during IR and IC have been performed via measurement [7] [8] [9] [10] [11]. Study of interventional radiology occupational exposures has also been made using the Monte Carlo (MC) technique [12] [13] [14]. This said, the stray radiation 3D distribution has not been previously obtained via MC simulation using the high definition reference Korean-man (HDRK-man) virtual anthropomorphic phantom [15]. Herein modeling has been made of staff exposure, the patient being imaged with a GE Infinia 3/8" machine, utilizing the versatile Geant4 toolkit [16]. The aim has been to study the effect of key parameters on occupational exposure distribution within the theatre. Specifically, the influence of kVp, field of view (FoV) and staff position has been investigated, focusing on three radiosensitive organs (lens of the eye, and lung and prostate).

2. Materials and Methods

Description is provided herein of the adopted methodology, presenting the voxelized phantom corresponding to the patient and staff, the X-ray imaging machine and X-ray tube output. Different proposed interventional imaging procedure scenarios are also outlined. We note that there are three phantom format types (stylized, voxel and hybrid) and four morphometric categories (reference, patient-dependent, patient-sculpted and patient-specific). Here we are limited to voxel type and reference category (patient matching by age only) to model phantoms.

2.1. Patient and Operator Modeling

In modeling patient and staff, close similarity has been noted between the ICRP
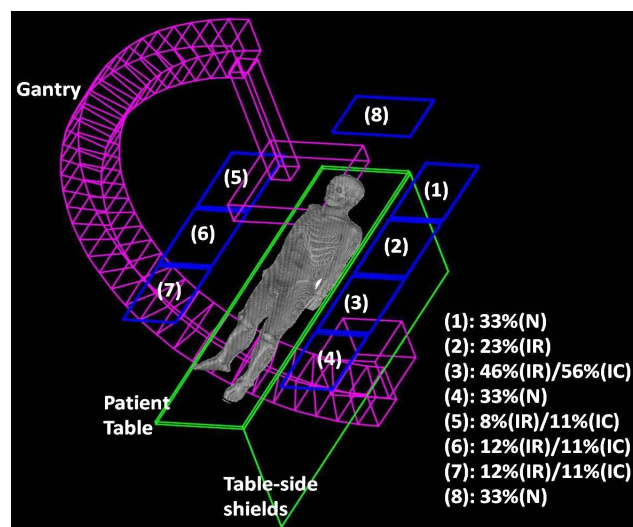
reference man and the voxelized phantom HDRK-man, including height and weight, a matter encouraging the use of the latter. Constructed from high-resolution photographic anatomical images, HDRK-man has a height of 171 cm and weight of 68 kg. Whereas, the ICRP models human having a height of 176 cm and weight of 73 kg. The considered phantom consists of some 30 million voxels, resolution $1.981 \times 1.981 \times 2.0854$ mm^3, distributed along a 3D array of dimension $247 \times 141 \times 850$, along the x, y and z coordinate axes, respectively. The elemental composition and density of each voxel were obtained from ICRU 46 [17], defining some 40 tissues/organs.

2.2. Gamma Camera and X-Ray Spectra

The GE Infinia II 3/8" C-arm machine modeled in this study has an inner radius of 1m and is made from a sturdy, rigid foam material (density 0.7 g/cm^3 and elemental composition of 50% H, 30% C, 10% N and 10% O). As shown in **Figure 1**, the gantry supports a CsI flat panel imager ($48 \times 48 \times 10$ cm^3) positioned close to the upper surface of the patient, while the under-couch X-ray tube is contained in an iron shielding surround. The couch is a $45 \times 190 \times 1.5$ cm^3 table made of PMMA material. A typical beam-hardening Pb sheet of 0.5 mm thickness has been added to the patient table in front of the primary X-ray beam. In generating the X-ray tube outputs, as modified by the particular choice of total filtration and parameter selection (kVp and mAs), use was made of the software known as spektr [18].

2.3. Irradiation Scenarios

The parameters studied during this work were as follows:

(1): 33%(N)
(2): 23%(IR)
(3): 46%(IR)/56%(IC)
(4): 33%(N)
(5): 8%(IR)/11%(IC)
(6): 12%(IR)/11%(IC)
(7): 12%(IR)/11%(IC)
(8): 33%(N)

Figure 1. Simulated experimental set-up, including the C-arm machine (Gantry, X-ray tube holder, CsI flat panel) and the HDRK-Man phantom lying on a table shielded with 0.5 mm Pb on its left side. Also shown: the eight most likely occupied locations by staff (Interventional Radiologist (IR), Interventional Cardiologist (IC) and Nurse (N)) with their occurrence (in %) during an interventional procedure.

- X-ray photon spectra: 60 kVp (Half Value Layer (HVL) = 2.3 mm Al), 80 kVp (HVL = 3.2 mm Al) and 120 kVp (HVL = 4.3 mm Al)
- C-arm orientation (fixed): vertical
- Exposure and patient orientation: postero-anterior (PA), lying on the bed
- Irradiated body area (denoted as FoV) (four values): 15 × 15, 20 × 20, 25 × 25, and 30 × 30 cm^2, centered at chest
- Staff locations (eight values): about 40 cm around the patient table, as proposed in literature [19] and shown in **Figure 1**
- Table height (fixed): 75 cm

2.4. Simulation and Data Collection

For MC simulation, use has been made of the Geant4 version 10.3 multithreaded mode [16] [20]. In respect of the large number of voxels representing the patient, utilization has been made of the nested parameterization provided for by the G4VNested Parameterization class. For the simulated X-ray room, a particular typical example of dimension 4.8 × 6.4 × 2.89 m^3 was chosen. Spectra generated through use of the spektr software have been included in the Geant4-based program, the inverse transform method being used to randomly generate the corresponding energies. Such method consisting of the sampling of random numbers from a given probability distribution function, uses the inverse cumulative distribution defined by the calculation of the cumulative integration for a given set of samples. For all cases, a pyramidal-shaped primary beam has been assumed, emanating from a point-like X-ray source towards the chest of the patient. In allowing simulation of the spatial distribution of the stray radiation, the room space was subdivided into 80 × 80 × 34 air-filled boxes, each of the dimension 5 × 5 × 5 cm^3. The scenario allows for scattered radiation evaluation up to 2 m away from the centre of the irradiation field. For a given choice of set-up, simulation has been made to obtain the air kerma free-in-air within air-filled boxes of the dimensions 10 × 10 × 10 cm^3, evaluated at the level of the lens of the eye, lung and prostate, at 165, 150 and 84 cm directly above the floor respectively. In order to obtain the parameter ESAK, simulation was made of the absorbed dose evaluated within 10 × 10 × 1 cm^3 air-filled boxes inserted directly under the patient table; this allows X-ray backscattering to be taken into account. All simulations were carried out on a Dell Precision T7610 workstation with 40 cores, equipped with an Intel Xeon E5-2680v2 CPU at 2.80 GHz and 256 GB RAM, working on the Linux operating system (Ubuntu 14.04). The number of generated primary particles was 5 × 10^8 (allowing statistical uncertainty of <3%) for all cases, with run times ranging from 8500 s to 17560 s (*i.e.* from 2.4 hours up to just below 5 hours).

3. Results and Discussion

Results and analysis are provided herein, concerning the three dominating parameters modifying the 3D stray radiation dose distribution, kVp, FoV and staff

location, evaluated at the level of the eyes, lung and prostate.

3.1. Effect of kVp

To assess the influence of kVp on the simulated scattered radiation distributions, comparison has been made of three cases: 120 kVp (HVL = 4.3 mm Al), 80 kVp (HVL = 3.2 mm Al) and 60 kVp (HVL = 2.3 mm Al) for a fixed value of FoV. Figures 2-4 provide dose maps at the particular organ levels. In changing the kVp from 60 to 80 to 120, the distribution of stray radiation is seen to progressively concentrate around the irradiated area of the patient.

Such results are in accord with literature [10] and theory, the latter depicted in Figure 5 showing polar plots of the Compton scattering cross-section as a function of energy [21], the forward direction becoming increasingly favored. Table 1 illustrates the ratios of air kerma free-in-air to entrance surface air kerma (ESAK), namely the scatter fraction, quoted in $\mu Gy/Gy \cdot cm^2$ [22], for all combinations of the eight staff locations, organ levels, FoV and spectral influence of kVp. As previously mentioned, observation is made of an inverse proportionality between ESAK and kVp. Moreover, in changing the kVp from 60 to 80 and from 80 to 120, keeping the FoV fixed, the scatter fraction is observed to approximately double, remaining almost constant for the three organ levels and the eight staff locations.

This can be rationalized to be due to the penetration and scattering abilities characterizing the spectral X-ray beam. Given the limited number of interventional scenarios studied, including the overall shape of the phantom, the choice
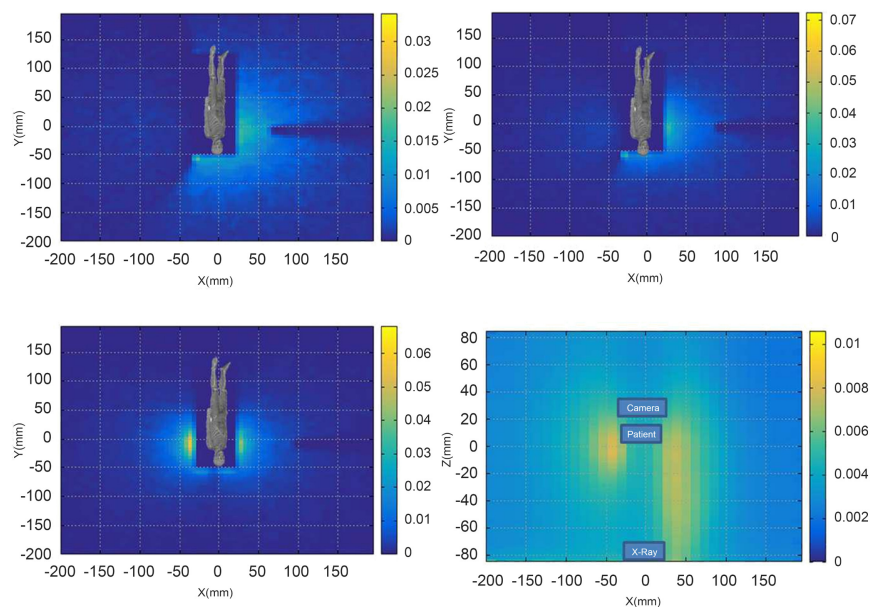
Figure 2. Simulated stray radiation obtained at 120 kVp (4.3 mm Al) and 30 cm FoV. Shown are dose maps for three horizontal plans, corresponding to eye lens (top left), lung (top right) and prostate (bottom left) levels; a vertical plan perpendicular to the C-arm gantry is shown at the bottom right. The colour bar indicates the relative strength of scattered radiation, from lowest values at the blue end to yellow at the upper end of the scale.
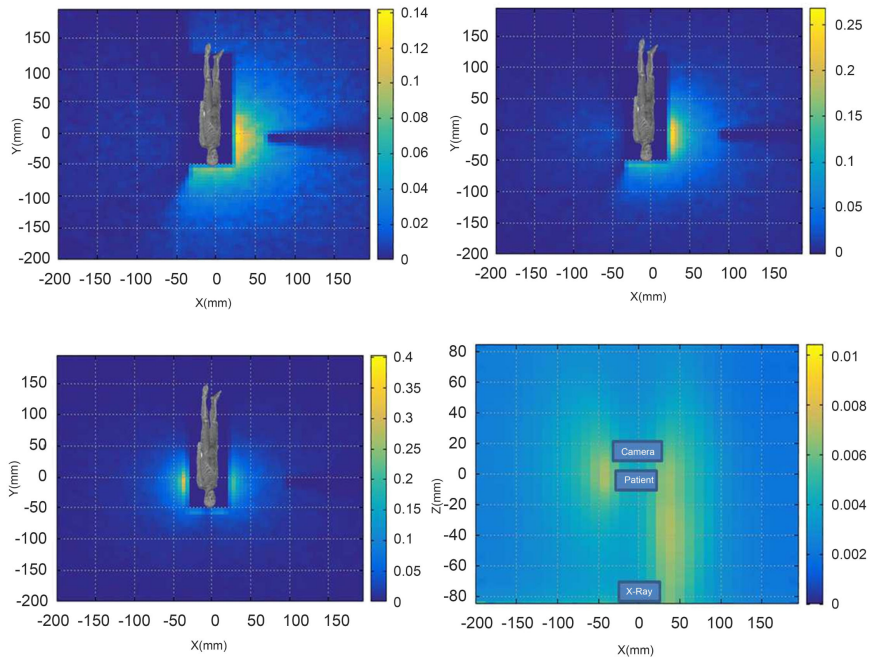
Figure 3. Simulated stray radiation obtained at 60 kVp (2.3 mm Al) and 30 cm FoV. Dose maps are shown for three horizontal plans at the level of the lens of eye (top left), lung (top right) and prostate (bottom left); a vertical plan normal to the C-arm gantry is shown at the bottom right.
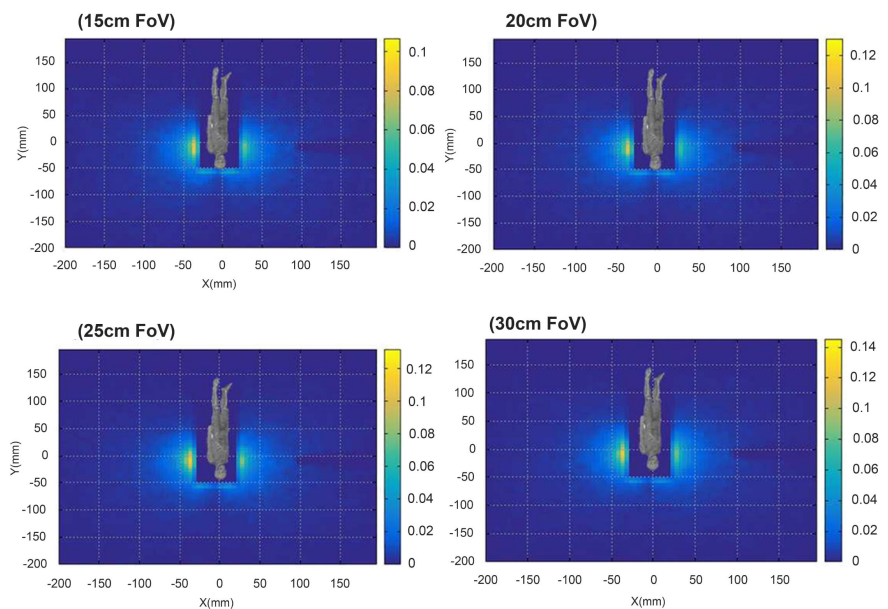
Figure 4. Simulated stray radiation obtained at 80 kVp (3.2 mm Al) corresponding to the horizontal patient level when varying the FoV from 15 cm (top left) to 30 cm (bottom right).

of C-arm machine and buildup specifications, the findings are not to be generalized. Nevertheless, while each interventional procedure will undoubtedly produce its own scattered radiation distribution, the current study can be considered to provide a good estimation of the overall situation.
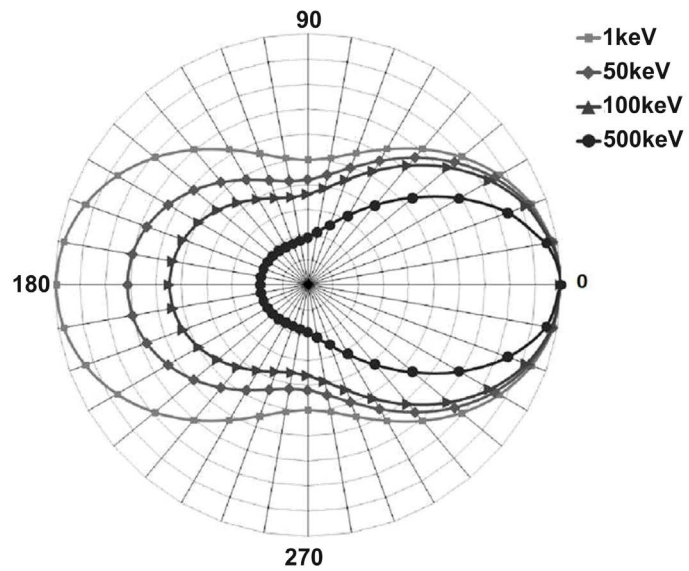
Figure 5. Klein-Nishina differential cross-sections as a function of the scattering angle and incoming photon energies.

Table 1. Simulated scatter fractions (in μGy/Gy·cm²) at the level of the lens of the eye, and lung and prostate, also the ESAK values. Data are given for all possible combinations of kVp (60, 80 and 120) and FoV (15, 20, 25 and 30 cm). The eight most likely occupied locations (Loc.) were emphasized. Cells highlighted in gray correspond to the radiological safe side.

Loc.	FoV/Z (cm)	60 kVp				80 kVp				120 kVp			
		15	20	25	30	15	20	25	30	15	20	25	30
1	165	1.1	0.8	3.2	7.1	2.3	2.3	4.3	5.2	1.6	2.7	2.6	3
	150	28.1	29.1	29	30.9	40.5	36.7	37.8	27.4	42.2	37.7	34.5	37.7
	84	26.1	25.6	23.6	29.8	55.8	49.4	58.9	52.5	56.9	60.2	63.3	55.9
	Sum	55.2	55.4	55.8	67.7	98.6	88.4	101	85.1	100.7	100.7	100	96.6
2	165	1.5	2.2	4.5	5.8	2.9	2	4.7	6.3	1.8	0.1	3.8	10.4
	150	31.4	29	30	31.4	49	38.8	40.1	36.3	38.9	41.4	42.8	43.2
	84	34.2	33.3	33.4	36.3	59.7	68.1	69.6	65.8	77.2	73.9	69.8	82.8
	Sum	67	64.5	67.8	73.5	111.7	108.9	114.5	108	117.9	115.4	116	136.4
3	165	2.3	4.1	8.8	8	4.8	6.2	9.4	12.3	2.9	7.1	7.9	8.1
	150	18.2	16.9	15.2	14.9	23.9	21.8	18.9	20.3	25.1	22	21.5	22.6
	84	15	11.5	10.1	15	33.3	32	23.8	23	22.2	23.3	29.9	33.4
	Sum	35.5	32.5	34.1	37.9	62	60	52.1	55.6	50.2	52.4	59.3	64
4	165	6.2	6	8.9	7.6	11.9	11.1	6.4	7.7	10	12.9	11.2	12.9
	150	4.7	5.3	6.9	9.5	12.9	7.6	11.4	10.2	10.1	6.3	13	9.1
	84	6.8	4.8	3.7	4.1	13	7.5	7.7	6.6	15.9	6.3	12.2	11.7
	Sum	17.7	16.2	19.6	21.2	37.8	26.2	25.5	24.5	36.1	25.4	36.3	33.7
5	165	0.9	2.7	2.7	6.7	2.9	4.1	5.4	7	2.9	5.6	8	8.2

Continued

	150	21	22.6	26.2	32.1	36.9	34.5	36.6	33.1	42.3	42.2	27.7	30.8
	84	28.6	34.6	32.6	31	64	61.5	57	62.7	64.5	64.3	62.1	62.9
	Sum	50.5	59.9	61.5	69.8	103.7	100.1	99	103	109.7	112.1	97.8	101.9
	165	3.2	3.3	4.3	8.2	1.4	2.6	5	5.6	2.3	5.1	4	6.7
6	150	31.3	33.4	34.3	32.5	44	40.6	46	30.6	44.6	41.1	34.7	38.2
	84	39.6	33.1	37.3	43.4	68.4	72.3	64.8	70.8	86.1	75.8	82.4	82.1
	Sum	74	69.8	75.8	84.1	113.8	115.5	115.8	107	133	122	121	127
	165	2.9	3.5	7.8	7.5	4.6	5.6	5.5	11.3	2.3	6.6	10	8
7	150	18.7	18	17.8	19.3	26.4	26.6	23.2	16.8	20.1	21.8	25.8	18
	84	16.7	15.7	14.6	15.1	24.4	27.3	34.6	34.4	31.6	25.5	25.2	26.4
	Sum	38.3	37.2	40.1	41.9	55.3	59.5	63.3	62.5	54	53.9	61	52.3
	165	12.5	11.1	9.8	11.3	15	11.7	11.6	11.7	21.1	16	16.8	13.4
8	150	13.8	16.1	15.5	15.3	23.3	17.9	20.8	21.1	17.5	20.8	19.3	23.5
	84	17.5	13.8	13.6	14.2	25.1	22.7	23.6	27.5	24	23.5	36.9	24.8
	Sum	43.8	41	38.9	40.8	63.3	52.3	55.9	60.3	62.7	60.3	73.1	61.7
	ESAK (nGy)	502.9	289.9	188.8	131.4	320.3	187.3	121.1	86.2	277.7	161.5	105	74.3

3.2. Effect of the FoV

In the example case of 80 kVp, stray radiation maps have been provided for particular likely FoV values of 15, 20, 25 and 30 cm. Horizontal plans corresponding to the patient table level are shown in Figure 4. No significant trend is discernible at this level, contrary to the ESAK and the scatter fraction distributions. In changing from a FoV of 15 to 30 cm, ESAK decreases continuously reaching values of a factor of three or better. Although limited to 80 kVp and to 14, 20 and 28cm circular shaped FoVs, Bethe *et al.* [23] found this to be an important effect on the stray radiation when changing the FoV parameter; the present work confirms their findings. Also supported is the trend towards near constancy of scatter fractions for a given value of kVp. Thus, we can generalize that the scatter fraction remains an almost constant function of the FoV for a fixed kVp parameter. This situation should be explored by extending the present study to take into account the effect of focal-to-skin and focal-to-detector distances.

3.3. Effect of Operator Location

The effect of changing staff location (as shown in Figure 1) on the scatter fraction at the level of the lens of the eye, lung and prostate is illustrated in Table 1. Despite buildup effects as observed in the measurements, applicability of the inverse square law has been confirmed, in terms of scattered fraction values, for the coupled staff locations of (1 and 5), (2 and 6) and (3 and 7). Moreover, we observe the typical times spent by the different members of staff (IR, IC and N) during an interventional procedure [19] to be optimal. This said, the present

study has been limited to the PA projection; further simulations would help, extending findings to other irradiation conditions of AP, LAO, RAO and such like.

4. Conclusion

There is an increasingly pressing need to quantify medical staff during interventional procedures. The present study, concerning scattered radiation from the patient and C-arm, has examined the influence of kVp, FoV and staff location on the 3D distribution and dose. Using an anthropomorphic voxelized phantom incorporated into a Geant4-based program, evaluation has been made of ESAK and scatter fraction at three organ levels of members of staff (eye lens, lung and prostate). For a given value of the FoV, ESAK is seen to increase with a decrease in kVp, supporting existing literature. Secondly, modification of kVp from 120 to 80 has a negligible effect (average deviation of 13.4%); conversely, in changing from 80 to 60 kVp an average decrease of 35.9% is found. Finally, the typically adopted locations of the various members of staff during interventions, in accordance with their roles, are found to be an optimal choice. From such findings, we urge the implementation of appropriate in-house protocols in seeking to mitigate the potential deleterious effects of radiation on members of staff.

Conflicts of Interest

The author declares no conflicts of interest regarding the publication of this paper.

References

[1] Cousins, C., et al. (2013) ICRP Publication 120: Radiological Protection in Cardiology. Annals of the ICRP, **42**, 1-125. https://doi.org/10.1016/j.icrp.2012.09.001

[2] Zakeri, F., Hirobe, T. and Akbari, N.K., (2010) Biological Effects of Low-Dose Ionizing Radiation Exposure on Interventional Cardiologists. Occupational Medicine (London), **60**, 464-469. https://doi.org/10.1093/occmed/kqq062

[3] Roguin, A., Goldstein, J., Bar, O. and Goldstein, J. A. (2013) Brain and Neck Tumors among Physicians Performing Interventional Procedures. American Journal of Cardiology, **111**, 1368-1372. https://doi.org/10.1016/j.amjcard.2012.12.060

[4] Bogaert, E., Bacher, K. and Thierens, H. (2008) A Large-Scale Multicentre Study in Belgium of Dose Area Product Values and Effective Doses in Interventional Cardiology Using Contemporary X-Ray Equipment. Radiation Protection Dosimetry, **128**, 312-323. https://doi.org/10.1093/rpd/ncm379

[5] Faulkner, K., Vano, A., Ortiz, P. and Ruiz, R. (2000) Practical Aspects of Radiation Protection in Interventional Radiology. IRPA-10 Proceedings of the 10th International Congress of the International Radiation Protection Association on Harmonization of Radiation, Human Life and the Ecosystem, Japan Health Physics Society, 7-16.

[6] Fardid, R., Mirzadeh, F. and Rezaei, H. (2017) Occupational Doses of Cardiologists in Cath Labs and Simulation Method. Journal of Cancer Research and Therapeutics, **13**, 901-907.

[7] Baptista, M., et al. (2015) Assessment of the Occupational Exposure in Real Time

during Interventional Cardiology Procedures. *Radiation Protection Dosimetry*, **165**, 304-309. https://doi.org/10.1093/rpd/ncv052

[8] Toossi, M., *et al.* (2015) Preliminary Results of an Attempt to Predict over Apron Occupational Exposure of Cardiologists from Cardiac Fluoroscopy Procedures Based on DAP (Dose Area Product) Values. *Australasian Physical & Engineering Sciences in Medicine*, **38**, 8391. https://doi.org/10.1007/s13246-014-0326-1

[9] Kong, Y., *et al.* (2015). Influence of Standing Positions and Beam Projections on Effective Dose and Eye Lens Dose of Anaesthetists in Interventional Procedures. *Radiation Protection Dosimetry*, **163**, 181-187. https://doi.org/10.1093/rpd/ncu148

[10] Loy Rodas, N. and Padoy, N., (2015) Seeing Is Believing: Increasing Intraoperative Awareness to Scattered Radiation in Interventional Procedures by Combining Augmented Reality, Monte Carlo Simulations and Wireless Dosimeters. *Journal of CARS*, **10**, 1181-1191. https://doi.org/10.1007/s11548-015-1161-x

[11] Toutaoui, K.N., *et al.* (2016) Assessment of Radiation Protection of Patients and Staff in Interventional Procedures in Four Algerian Hospitals. *Radiation Protection Dosimetry*, **168**, 55-60. https://doi.org/10.1093/rpd/ncv001

[12] Siiskonen, T., Tapiovaara, M., Kosunen, A., Lehtinen, M. and Vartiainen, E. (2007) Monte Carlo Simulations of Occupational Radiation Doses in Interventional Radiology. *The British Journal of Radiology*, **80**, 460-468. https://doi.org/10.1259/bjr/26692771

[13] Koukoravaa, C., Carinou, E., Ferrari, P., Krim, S. and Struelens, L. (2011) Study of the Parameters Affecting Operator Doses in Interventional Radiology Using Monte Carlo Simulations. *Radiation Measurements*, **46**, 1216-1222. https://doi.org/10.1016/j.radmeas.2011.06.057

[14] Santos, W.S., *et al.* (2015) Exposures in Interventional Radiology Using Monte Carlo Simulation Coupled with Virtual Anthropomorphic Phantoms. *Physica Medica*, **31**, 929-933. https://doi.org/10.1016/j.ejmp.2015.06.011

[15] Kim, C.H., *et al.* (2008) HDRK-Man: A Whole-Body Voxel Model Based on High-Resolution Color Slice Images of a Korean Adult Male Cadaver. *Physics in Medicine & Biology*, **53**, 4093-4106. https://doi.org/10.1088/0031-9155/53/15/006

[16] Allison, J., *et al.* (2016) Recent Developments in GEANT4. *Nuclear Instruments and Methods in Physics Research A*, **835**, 186-225. https://doi.org/10.1016/j.nima.2016.06.125

[17] White, D.R., Griffth, R.V. and Wilson, I.J. (1992) Photon, Electron, Proton and Neutron Interaction Data for Body Tissues. *Journal of the International Commission on Radiation Units and Measurements*, **os24**, Report 46.

[18] Punnoose, J., Xu, J., Sisniega, A., Zbijewski, W. and Siewerdsen, J.H. (2016) Technical Note: Spektr3.0—A Computational Tool for X-Ray Spectrum Modeling and Analysis. *Medical Physics*, **43**, 4711-4717. https://doi.org/10.1118/1.4955438

[19] Efstathopoulos, E.P., *et al.* (2011) Occupational Radiation Doses to the Extremities and the Eyes in Interventional Radiology and Cardiology Procedures. *The British Journal of Radiology*, **84**, 70-77. https://doi.org/10.1259/bjr/83222759

[20] Cosmo, G. and the Geant4 Collaboration (2014) Geant4—Towards Major Release 10. *Journal of Physics: Conference Series*, **513**, Article ID: 022005. https://doi.org/10.1088/1742-6596/513/2/022005

[21] Klein, O. and Nishina, Y. (1994) On the Scattering of Radiation by Free Electrons According to Dirac's New Relativistic Quantum Dynamics. In: Bethe, H.A. and Guth, A.H., Eds., *The Oskar Klein Memorial Lectures, Vol. 2: Lectures*, World

Scientific Publishing, Singapore, 113-139.
https://doi.org/10.1142/9789814335911_0006

[22] ICRU (2005) Patient Dosimetry for X-Rays Used in Medical Imaging, 2005. ICRU Report No. 74, International Commission on Radiation Units and Measurements, Bethesda.

[23] Bethe, A.S., *et al*. (2006) An Investigation of Operator Exposure in Interventional Radiology. *Radiographics*, **26**, 1533-1541. https://doi.org/10.1148/rg.265055127